JOURNAL OF SOLID STATE CHEMISTRY 119, 147–156 (1995)

Crystal Structures, Chemical Reactivity, Magnetic Properties, and Mössbauer Spectroscopy of the Quasi-Ternary Channel Compounds $TlV_{5-y}Fe_yS_8$ ($y = 0.5 - 1.5$)

W. Bensch and O. Helmer

Institut für Anorganische Chemie, Universität Frankfurt, Marie-Curie-Str. 11, D-60439 Frankfurt a.M., Germany

J. Lu, H.-J. Hesse, G. Wortmann

FB Physik, Universität-GH Paderborn, D-33095 Paderborn, Germany

and

M. Kraus and K. Lüders

Institut für Experimentalphysik, Freie Universität Berlin, Arnimallee 14, D-14195 Berlin, Germany

Received December 27, 1994; in revised form March 27, 1995; accepted March 28, 1995

Single crystal X-ray investigations reveal that the unit cell volume of $TlV_{5-y}Fe_yS_8$ increases with increasing Fe content. This unusual and unexpected behavior is explained with the increasing metal-to-metal distances as a function of Fe abundance. Tl-poorer samples can be obtained with a topotactical redox reaction using iodine in donor solvents. During this reaction the host material is strongly attacked by the redox agent. The magnetic properties can be explained on the basis of the coexistence of a temperature-independent Pauli paramagnetism (TIP) and a Curie–Weiss-like contribution from localized magnetic moments. With raising Fe abundance the effective magnetic moment per Fe is reduced and an increase of the value for the TIP is observed. This is indicative of strong delocalization of metal $3d$ electron density as a function of Fe abundance. The effective magnetic moment per Fe points to Fe^{3+} in the low spin state ($S = \frac{1}{2}$). This is further supported by Mössbauer experiments. The Fe atoms are distributed on the three possible crystallographic sites with a preference for the $M2$ site. The isomer shifts as well as the quadrupole splittings are indicative of Fe^{3+} in the low spin state. A local effective Debye temperature of 260(3) K was evaluated for the Fe^{3+} ions, suggesting no significant differences of the stiffness of the compounds. For TlV_4FeS_8 and $TlV_{4.5}Fe_{0.5}S_8$ below about 20 and 10 K, respectively, an ordering of the localized electronic spins is observed, leading to a broadening of the spectra. The change of the internal magnetic fields with temperature does not follow the Brillouin function for $S = \frac{1}{2}$, suggesting a spin-glass behavior.

1. INTRODUCTION

The crystal structure of ternary chalcogenides with the formal composition AM_5X_8 consists of layers of edge-sharing distorted MX_6 octahedra parallel to the 001 plane. Double units of MX_6 octahedra with common edges connect these layers via common faces parallel to the crystallographic b-axis. The resulting 3-dimensional network contains nearly rectangular channels parallel to the b-axis. The A atoms are confined within these channels. The connection of the MX_6 octahedra via common edges and faces results in the formation of relatively short metal-to-metal distances and hence interesting physical properties.

The magnetic behavior of a number of compounds with the TlV_5S_8-type structure is well documented (1–5). The pure V compound is a metal and shows the coexistence of a temperature-dependent Curie–Weiss-like paramagnetism with a temperature-independent Pauli paramagnetism (TIP) (1). The magnetic moment on the V atoms is small and significantly lower than the spin-only moment expected for a V^{3+} (d^2) species. The crystal structure, the magnetic properties, and the electronic band structure are strongly influenced by the Tl concentration in $Tl_xV_5S_8$ (6). A study of the magnetic properties of compounds in which V is partially substituted by Ti, Cr, Mn, or Fe ($0 \leq y \leq 1$ in $TlV_{5-y}M_yS_8$) has shown that the magnetic moment per M atom does not exceed 40% of the theoretical value.

0022-4596/95 $12.00

The only exception was $Tl_{0.95}V_4FeS_8$, which showed a high magnetic moment indicative for a localization of the Fe 3*d* electrons (3). The successive substitution of V by Cr ($1 \leq y \leq 4$ in $TlV_{5-y}Cr_yS_8$) results in a decreasing metallic character and the occurrence of a complex magnetic behavior is observed (7). The magnetic properties of the pure Cr compound $TlCr_5S_8$ are dominated by the formation of strong antiferromagnetically coupled Cr_2 dimers. This compound is a semiconductor (5).

A large number of iron-substituted vanadium sulfides and selenides like FeV_2Se_4 (8), $V_{3-y}Fe_yS_4$ (9, 10), $V_{5-y}Fe_yS_8$ (10, 11), $V_xFe_{1-x}S$ (12), and $Li_xFe_yV_{1-y}S_2$ (13) have been investigated with Mössbauer spectroscopy and with respect to their magnetic properties. In most compounds Fe is exclusively introduced as Fe^{2+} in the high spin state. In $BaVS_3$ doped with 2% ^{57}Fe the iron atoms are in an Fe^{3+} low spin state (11). The possibility of a spin crossover as function of temperature was discussed for $V_{5-x}Fe_xS_8$ (11) and for $Fe_xTa_{1-x}S_2$ (14).

Within a formal "ionic" picture compounds with the composition AM_5X_8 can be formulated as $A^+M_5^{3+}S_8^{2-}$. Hence, it is expected that V is substituted by Fe^{3+}. The introduction of iron in the Fe^{3+} low spin state with an ionic radius of 0.55 Å should lead to a significant decrease of the crystallographic lattice parameters ($r(V^{3+}) = 0.64$ Å), whereas no significant changes are expected for Fe^{3+} in the high spin state ($r(Fe^{3+}) = 0.645$ Å).

The present contribution reports single crystal data for $TlV_{5-y}Fe_yS_8$ ($y = 0.5$, 1.0, and 1.5) as well as for a Tl-poor sample of TlV_4FeS_8. Results of ^{57}Fe Mössbauer experiments conducted between 1.7 and 300 K as well as results of the magnetic susceptibility measurements performed between 10 and 300 K are presented. In addition the chemical reactivity of the title compounds against the redox agent I_2 in acetonitrile is discussed.

2. EXPERIMENTAL

Mixtures of the elements with the desired stoichiometry were transferred within a glove box under an Ar atmosphere into a degassed silica ampoule. The ampoules were heated to 1273 K within 24 hr and held at this temperature for 1 day. Afterward the temperature was lowered to 1223 K within 24 hr and the ampoules were fired at this temperature for 10 days. Finally the mixtures were cooled down to room temperature with 100 K/h. The products consist of black needles with a metallic lustre. Small grey spherical precipitations were found in the top of the ampoules and were identified as unreacted Tl metal. All reflections of the X-ray powder patterns recorded with monochromatized Co$K\alpha$ radiation could be indexed on the basis of the monoclinic TlV_5S_8 structure type. Attempts to introduce more than one Fe in $TlV_{5-y}Fe_yS_8$ lead to inhomogeneous products with the minor impurity phase V_3S_4. Hence, magnetic experiments as well as Mössbauer investigations could be undertaken only with powdered samples of $TlV_{4.5}Fe_{0.5}S_8$ and TlV_4FeS_8. Nevertheless, single crystal X-ray experiments were performed for Tl $V_{5-y}Fe_yS_8$ with $y = 0.5$, 1.0, and 1.5. The iron content of the crystals used for single crystal investigations was determined with energy dispersive analysis of X-rays (EDAX). The determined iron content amounts to 0.47(3), 0.95(4), and 1.47(2) for $TlV_{4.5}Fe_{0.5}S_8$, TlV_4FeS_8, and $TlV_{3.5}Fe_{1.5}S_8$, respectively.

X-ray intensities were collected on a STOE AED II diffractometer using Mo$K\alpha$ radiation ($\lambda = 0.7107$ Å, graphite monochromator). Important technical details of the data collections as well as some refinement results are summarized in Table 1. Chemical redox reactions were undertaken with iodine in acetonitrile (0.5 mg/ml). The Tl and Fe content of the solutions and of the residues were determined with atomic absorption spectrometry (AAS). The magnetic susceptibilities were measured between 10 and 300 K on a SQUID (external magnetic field 300 G). Field dependence was checked at room temperature by varying the external field and was found to be neglibly small. The raw data were corrected for core diamagnetism. Mössbauer spectra were recorded between 1.7 and 300 K using ^{57}Co in Pd. The isomer shift was calibrated relative to metallic iron.

3. RESULTS AND DISCUSSION

3.1. Crystal Structure

The crystal structure of $TlV_{5-y}Fe_yS_8$ is displayed in Fig. 1. As a result of the edge- and face-sharing octahedra, short metal-to-metal distances are observed. The metal atom network is also depicted in Fig. 1 and can be described as double zigzag chains of *M*1 and *M*3 atoms within the 001 plane which are connected by single zigzag chains of *M*2 atoms parallel to the *b*-axis. Important interatomic distances are summarized in Table 2.

The Tl content of the single crystals was determined with a freely varying site occupation factor (sof) using the data sets corrected for absorption. This procedure leads to $Tl_{0.90(1)}V_{4.5}Fe_{0.5}S_8$, $Tl_{0.92(1)}V_4FeS_8$, and $Tl_{0.92(2)}V_{3.5}Fe_{1.5}S_8$.

Three different crystallographic sites are available for the metal atoms. Two are in the layers and one is in the double unit. Hence, the iron atoms may substitute the V atoms in a random way or may preferably occupy one or two of the sites. As expected, the differences in the scattering power of Fe and V are too small to distinguish between these two possibilities.

It is surprising that the *a*- and *c*-axes are only slightly affected by the substitution of V by Fe despite the smaller radius of Fe^{3+} compared to that of V^{3+}. It is also noteworthy that the *b*-axis exhibits a significant increase and the monoclinic angle shows a considerable decrease. These

TABLE 1
Technical Details of the Data Collection and Selected Refinement Results for $TlV_{5-y}Fe_yS_8$ (y = 0.5, 1.0, and 1.5) and $Tl_{0.62}V_4FeS_8(x)$

y	0.5	1.0	1.5	0	x
a[Å]	17.494(2)	17.500(2)	17.509(5)	17.504(6)	17.471(2)
b[Å]	3.318(1)	3.328(1)	3.338(1)	3.307(1)	3.299(1)
c[Å]	8.520(1)	8.518(1)	8.511(2)	8.521(2)	8.491(1)
β[°]	103.88(1)	103.73(1)	103.67(2)	104.00(3)	103.83(2)
V[Å^3]	480.1(1)	481.9(1)	483.3(1)	478.6(1)	475.2(3)
ΣI	1628	1636	1646		1612
Unique	815	818	823		806
N_0	684	706	763		472
N_p	46	46	46		46
w^a	0.00005	0.0004	0.0007		0.0003
x^b	0.00103(5)	0.00109(8)	0.0017(1)		0.0004(2)
R_{int}[%]	2.32	2.01	2.36		6.26
R[%]	1.94	2.16	2.57		4.91
Rw[%]	1.88	2.25	2.82		4.59
GOOF	1.13	0.99	1.069		1.433
δF [e/Å]	1.49	1.53	1.86		1.53
	−0.78	−1.08	−1.73		−1.85

Note. Data for TlV_5S_8 (y = 0) are given for comparison and were taken from Ref. (15).
[a] Weighting scheme: $w = 1/(\sigma^2(F) + w * F^2)$.
[b] Extinction correction: $F^* = F[1 + 0.002 * x * F^2/\sin 2\Theta)]^{-1/4}$.

changes result in larger unit cell volumes than that of the pure vanadium compound (15) (compare Table 2).

A closer inspection of the interatomic V/Fe–S separations reveals that the average ⟨M–S⟩ distances of the three different MS_6 octahedra are not affected. In contrast, appreciable alterations occur for the asymmetry of the octahedra which may be expressed by the difference δ between the largest (V/Fe)–S and shortest (V/Fe)–S distances (compare Table 2). There are two contradicting tendencies. The $M1$ and $M3$ centered octahedra become more symmetric with rising Fe content, whereas the asymmetry of the $M2$ centered octahedron increases with increasing Fe

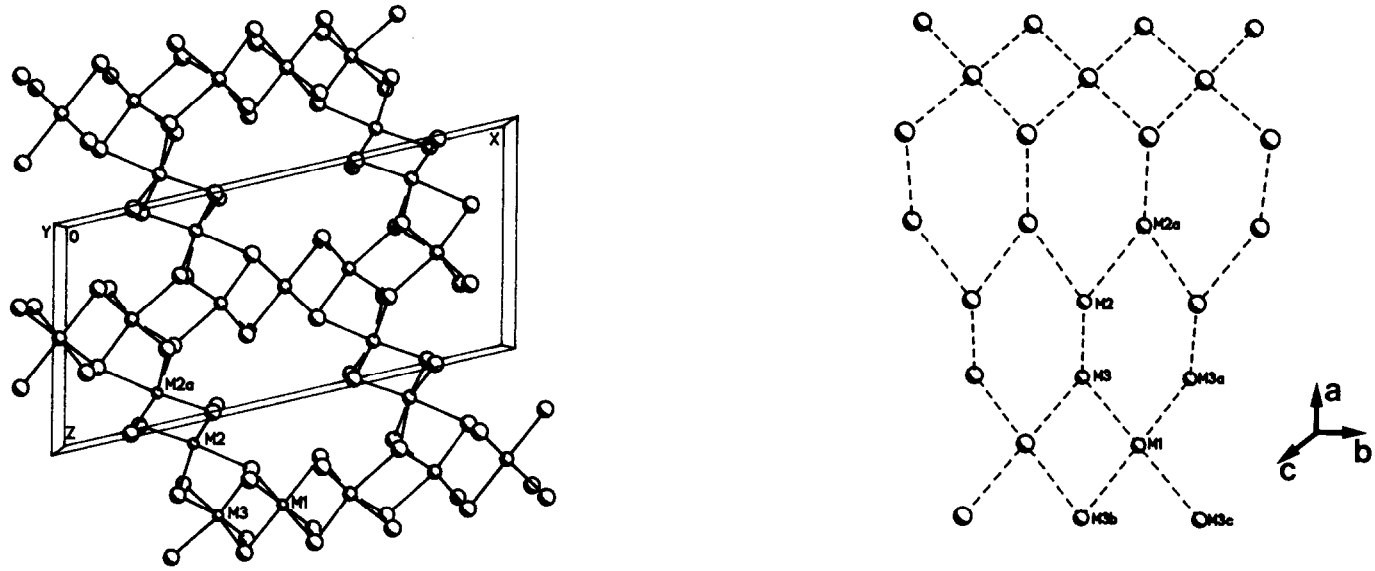

FIG. 1. The crystal structure of TlM_5X_8 (left) and the quasi-two-dimensional metal atom network (right). The Tl atoms are confined within the nearly rectangular channels parallel to the crystallographic b-axis (not shown).

TABLE 2
Selected Interatomic Distances [Å] for $TlV_{4.5}Fe_{0.5}S_8$, TlV_4FeS_8, $TlV_{3.5}Fe_{1.5}S_8$, and $Tl_{0.62}V_4FeS_8(x)$

y	0.5	1	1.5	0	x
Tl–S1 4×	3.270(1)	3.279(1)	3.286(1)	3.268(2)	3.257(3)
Tl–S2 4×	3.220(1)	3.229(1)	3.235(1)	3.212(2)	3.197(3)
Tl–S4 2×	3.318(1)	3.319(1)	3.321(1)	3.320(2)	3.300(4)
⟨Tl–S⟩	3.260	3.267	3.273	3.256	3.242
δ	0.098	0.090	0.086	0.108	0.103
*M*1–S2 2×	2.399(1)	2.395(1)	2.391(1)	2.402(2)	2.400(4)
*M*1–S4 4×	2.393(1)	2.392(1)	2.392(1)	2.391(1)	2.389(2)
⟨*M*1–S⟩	2.395	2.393	2.392	2.395	2.393
δ	0.006	0.003	0.001	0.011	0.011
*M*2–S1	2.295(1)	2.292(1)	2.292(1)	2.301(2)	2.287(4)
*M*2–S4	2.506(1)	2.525(1)	2.532(1)	2.490(2)	2.503(4)
*M*2–S1 2×	2.350(1)	2.344(1)	2.347(1)	2.352(2)	2.344(4)
*M*2–S3 2×	2.504(1)	2.510(1)	2.507(1)	2.495(2)	2.500(4)
⟨*M*2–S⟩	2.418	2.421	2.422	2.414	2.413
δ	0.211	0.233	0.240	0.194	0.216
*M*3–S3	2.536(1)	2.525(2)	2.520(2)	2.539(2)	2.539(5)
*M*3–S2 2×	2.328(1)	2.329(1)	2.327(1)	2.329(1)	2.318(3)
*M*3–S3 2×	2.486(1)	2.489(1)	2.494(1)	2.485(1)	2.486(3)
*M*3–S4	2.302(1)	2.305(2)	2.306(1)	2.302(2)	2.295(5)
⟨*M*3–S⟩	2.411	2.411	2.411	2.412	2.407
δ	0.234	0.220	0.214	0.237	0.244
*M*1–*M*3	3.129(1)	3.136(1)	3.142(1)	3.128(1)	3.107(2)
*M*2–*M*3	3.028(1)	3.040(1)	3.040(1)	3.013(2)	3.037(3)
*M*2–*M*2	3.023(1)	3.021(1)	3.029(1)	3.036(2)	2.999(4)

Note. Data for TlV_5S_8 ($y = 0$) are given for comparison (15).

abundance. In addition, considerable changes are observed for the metal-to-metal separations. The distances between the *M*2 atoms of the double unit and *M*1 and *M*3 within the sheets as well as between *M*2 and *M*3 (common face) are enlarged within the substitution series. These changes are indicative of altered *M*–S and *M*–*M* bonding interactions and suggest less strong bonds between the different metal atoms. The alterations of the bonding interactions are responsible for the observed unusual changes of the lattice parameters.

Using the ionic radii for V^{3+} (0.640 Å) and Fe^{3+} (0.645 Å for high spin and 0.55 Å for low spin) reported by Shannon (16), the observed changes of the interatomic separations indicate that iron is introduced as Fe^{3+} in the high spin state. It is noted that the use of ionic radii given for sulfides (17) leads to the same conclusion ($r(V^{3+}) = 0.72$ Å, $r(Fe^{3+})_{hs} = 0.72$ Å, $r(Fe^{3+})_{ls} = 0.595$ Å). But, as is shown in subsections 3.3 and 3.4, the V ions are replaced by Fe^{3+} in the low spin state.

The reduction of the Tl content to $x = 0.62$ in $Tl_xV_4FeS_8$ leads to a pronounced anisotropic shrinkage of the lattice parameters with the largest change for the *b*-axis (reduction by about 0.6%). The changes are reflected by distinct alterations of the interatomic separations and of the asymmetry of the MS_6 octahedra as well as of the TlS_{10} bicapped distorted cube. Whereas the *M*2 centered octahedron becomes more symmetric compared to the Tl-rich sample, the *M*1 and *M*3 centered octahedra are more irregular. In addition, the average ⟨*M*2–S⟩ distance is reduced, whereas the average ⟨*M*–S⟩ distances for *M*1 and *M*3 are only slightly affected by the reduction of the Tl content (compare Table 2). A pronounced reduction occurs also for the *M*1–*M*3 and *M*2–*M*2 interatomic separations (*M* atoms in octahedra connected by common edges), whereas the *M*2–*M*3 (across common face) distance remains unchanged. The individual and average ⟨Tl–S⟩ interatomic contacts are significantly shorter in the Tl-poorer sample. These anisotropic alterations of the interatomic interactions may be the result of geometrical and electronic factors. A pure geometrical effect due to the partial depletion of the channel should result in isotropic changes of the lattice parameters and interatomic separations. But, if the formal description of TlM_5X_8 as composed of a negatively charged host lattice $[M_5X_8]^-$ and a guest ion Tl^+ is accepted, the decrease of the Tl concentration in $Tl_xV_4FeS_8$ must result either in the partial oxidation of Tl^+ to Tl^{3+} or in the oxidation of some of the M^{3+} ions to M^{4+} ions. From the above mentioned changes of the interatomic separations it is suggested that some of the M^{3+} ions are oxidized. This conclusion is further supported by our results of photoemission experiments obtained on $Tl_xV_5S_8$ which gave no evidence for a Tl^{3+} species but exhibited significant changes of the V 2*p* core level spectra (6). At the end, it is noted that similar changes of the interatomic separations were also observed for $Tl_xV_5S_8$ (6) and $Tl_xCr_5Se_8$ (18).

3.2. Chemical Reactivity

It is well documented that nonstoichiometric compounds with the formal composition $A_xM_5X_8$ can be obtained by a topotactical redox reaction using iodine or bromine in donor solvents like CH_3CN (15, 19). The lower phase limit for $Tl_xV_5S_8$ was reported to be $x = 0.33$ (2).

The change of the Tl content with time for the title compounds is displayed in Fig. 2. Within the first 2 days about 50% of the Tl is removed. After 11 days the nominal composition $Tl_{0.2}V_{5-y}Fe_yS_8$ is reached. Since the mass loss was larger than expected, the iron content within the solution was also determined. The change of the Fe content with time is also shown in Fig. 2. As can be seen during the first 2 days the loss of Fe is negligibly small. But after 11 days about 20% of the initial Fe is also removed. This observation strongly suggests that iodine not only reacts with Tl but also attacks the host matrix. This

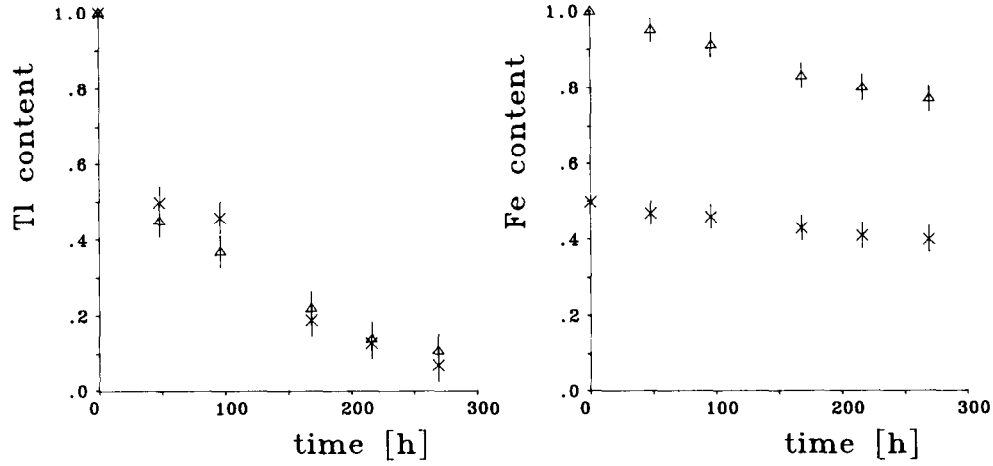

FIG. 2. The change of the Tl content (left) and Fe content (right) as a function of time during the topotactic redox reaction of $Tl_xV_{5-y}Fe_yS_8$. (×) y = 0.5; (Δ) y = 1.0.

is further shown by SEM micrographs taken after the redox reaction. While as-grown crystals exhibit a smooth surface without any unusual features, the crystals show after the reaction deep cracks parallel and perpendicular to the crystallographic *b*-axis (see Figs. 3a and 3b) indicative of a reaction between the host material and the iodine. It must be stressed here that in pure TlV_5S_8 the host material is not attacked by I_2 (20).

3.3. Magnetic Properties

The temperature dependence of the inverse magnetic susceptibilities for the two compounds is displayed in Fig.

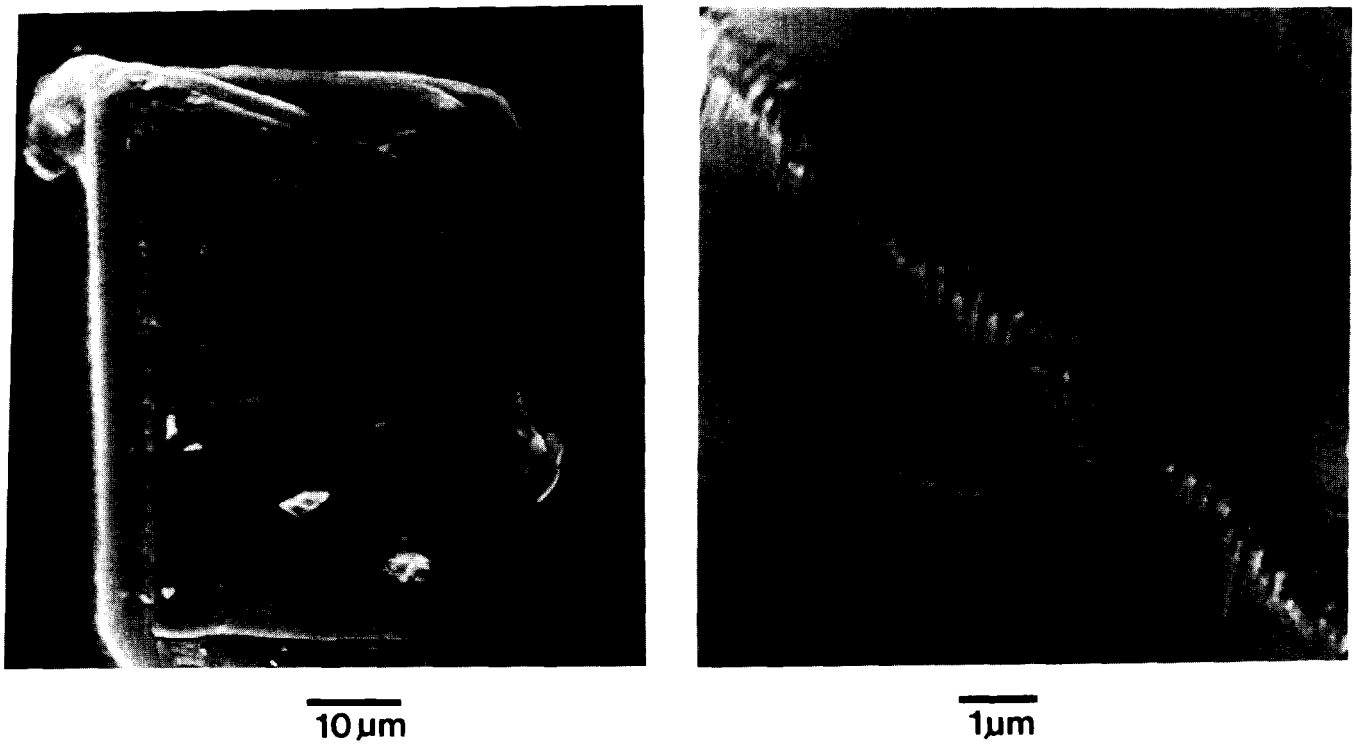

FIG. 3. SEM micrographs of single crystals of TlV_4FeS_8 taken after the reaction with iodine in CH_3CN after 11 days reacting time.

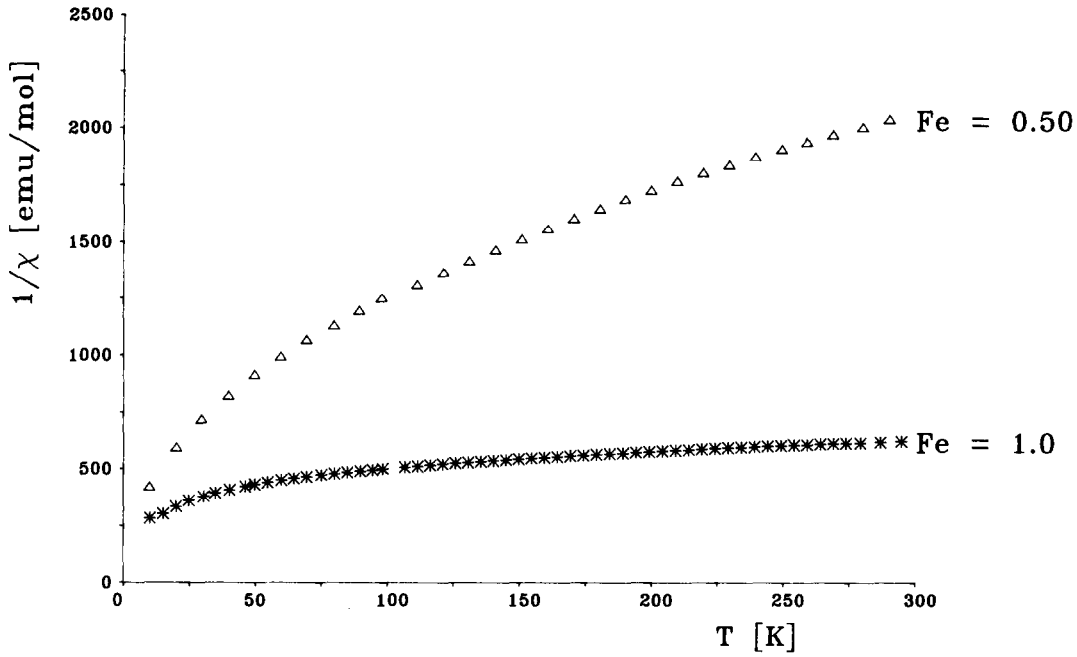

FIG. 4. The temperature dependence of the inverse magnetic susceptibilities of (Δ) $TlV_{4.5}Fe_{0.5}S_8$ and (*) TlV_4FeS_8.

4. The data were fitted between 30 and 300 K with an equation which accounts for a temperature-independent paramagnetism due to delocalized electrons and a Curie–Weiss law due to localized magnetic moments:

$$\chi(T) = \chi(\text{TIP}) + C/T - \Theta.$$

The numerical results as well as magnetic data of selected iron-containing compounds are listed in Table 3. If only Fe atoms contribute to the magnetic moment in $TlV_{4.5}Fe_{0.5}S_8$ the μ_{eff} per Fe atom of 2.29 μ_B is higher than the spin-only (s.o.) value expected for Fe^{3+} in the low spin state (μ = 1.73 μ_B). Hence, it is suggested that either a not fully quenched orbital momentum contributes to the enhanced effective magnetic moment or localized V 3*d* electrons contribute to the effective magnetic moment. For the Fe-richer sample we obtained a significantly lower μ_{eff}/Fe of 1.89 μ_B which is also larger than the s.o. value expected for low spin Fe^{3+}. If both V and Fe atoms contribute to μ_{eff}, the evaluated magnetic moment per *M* atom reaches only about 25% of the expected value of 2.53 μ_B.

It is noted that the χ(TIP) rises by a factor of about 4.7 when the Fe abundance is increased from 0.5 to 1 per formula unit. This observation together with the fact that the magnetic moment per Fe atom is significantly reduced in the Fe-richer sample indicates that the V 3*d* electron density is fully delocalized in TlV_4FeS_8 and partially localized in the Fe-poorer compound. But there are also hints that Fe 3*d* electron density is partially delocalized. For the χ(TIP) of the pure ternary vanadium sulfide a value

TABLE 3
Magnetic Data for $TlV_{4.5}Fe_{0.5}S_8$ and TlV_4FeS_8

	χ(TIP) [10^{-3} emu/mol]	μ/Fe	μ/M	θ	Ref.
$TlV_{4.5}Fe_{0.5}S_8$	1.45	2.29	0.72	−31(2)	this work
TlV_4FeS_8	6.95	1.89	0.85	−42(2)	this work
$Tl_{0.95}V_4FeS_8$	2.42	2.05		−65.6	3
$Fe_{0.84}Ni_{0.16}Te_{1.57}$	—	5.66		—	22
$Fe_{0.90}Ni_{0.1}Te_{1.57}$	—	5.34		—	22
$FeTe_{1.57}$	—	6.15		—	22
$Fe_{0.96}Se$	—	4.98[a]		−792	23
$Fe_{0.75}Se$	—	5.58[a]		−2223	23
FeV_2S_4	—	3.40		−115	24
FeV_2Se_4	—	3.33		−122	24
$FeTi_2Se_4$	—	3.61		10	24
$FeTi_2S_4$	—	3.51		125	24
$FeTi_2Se_4$	—	4.15		—	25
FeV_2S_4	—	4.15		—	25
FeV_2Se_4	—	4.18		—	25
FeV_2S_4	—	3.2		—	21
$Fe_{1.8}V_{1.2}S_4$	—	2.61		—	21
Fe_2VS_4	—	1.8		—	21
$Fe_{0.25}V_{0.75}S_2$	—	0.7		5	13
$Fe_{0.5}V_{0.5}S_2$	—	1.2		30	13
$LiFe_{0.25}V_{0.75}S_2$	—	3.2		35	13

Note. Data for different iron containing compounds are listed for comparison.

[a] The μ/Fe results from Fe^{2+} (d^6) and Fe^{3+} (d^5).

of about 2×10^{-3} emu/mole was reported (3), which is slightly larger than the value obtained for $TlV_{4.5}Fe_{0.5}S_8$. If one V is replaced by one Fe and if only the V $3d$ electrons are delocalized, one would expect a further reduction of the χ(TIP), in contrast to our observation. Hence, it can be assumed that both V $3d$ and Fe $3d$ electron density contribute to the χ(TIP). A delocalization of Fe $3d$ electron density was also postulated for the Fe-richer members of the solid solution $V_{3-x}Fe_xS_4$ (21).

Since the Fe–Fe distances (compare Table 2) seem to be too long for strong direct exchange interactions (Fe–Fe in Fe metal: 2.52 Å), the possibility of the formation of antiferromagnetically coupled Fe_2 dimers which would explain the lowering of the effective magnetic moment as well as the high value for the TIP is excluded.

To further support the above-mentioned result that the χ(TIP) of TlV_4FeS_8 is larger than that of the Fe-poorer sample we measured the electrical resistivity of different single crystals parallel to the needle axis which coincides with the crystallographic b-axis. The room temperature resistivity of a single crystal of $TlV_{4.5}Fe_{0.5}S_8$ amounts to about 650 $\mu\Omega$ cm and for TlV_4FeS_8 we obtained about 350 $\mu\Omega$ cm. Unfortunately, the crystals are very thin ($d < 0.02$ mm) and the measured thickness is subject to a large uncertainty.

The negative sign of the Weiss constant is indicative of antiferromagnetic exchange interactions and these interactions seem to be more pronounced in the Fe-richer sample. But down to 10 K no ordering of the magnetic moments could be observed.

The magnetic properties of a sample with the composition $Tl_{0.95}V_4FeS_8$ was reported by (3). The magnetic data are somewhat at variance with the results obtained during the present study. The differences may be due to the significantly different preparation procedures. The lower annealing temperature employed in the study of (3) seems to lead to an exclusive occupation of only one of the three possible crystallographic metal sites (see Mössbauer data published in (3)).

3.4. *Mössbauer Spectroscopy*

Typical Mössbauer spectra of $TlV_{5-x}Fe_xS_8$ with $x = 0.5$ and 1.0 taken at 77 K are displayed in Fig. 5. The spectra are well described by the superposition of three different quadrupole doublets due to the three different crystallographic metal ($M1$–$M3$) sites. The derived hyperfine parameters and site intensities are listed in Table 4. Hyperfine field data for different iron-containing compounds extracted from the literature are summarized in Table 5.

Both spectra exhibit a dominant doublet with the largest quadrupole splitting (QS = 0.97 mm/sec at 77 K) with 63% ($x = 0.5$) and 58% ($x = 1.0$) of the spectral area. From this and the varying intensities of the two other doublets, as reflected by the change in spectral appear-

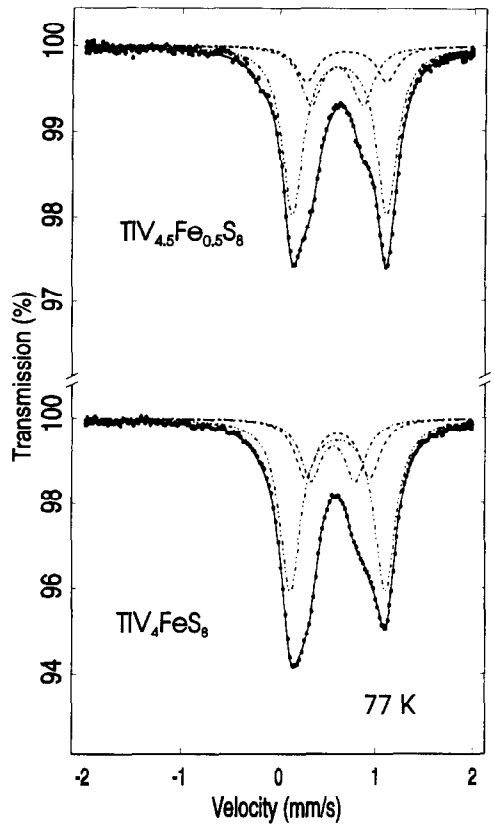

FIG. 5. Mössbauer spectra of $TlV_{4.5}Fe_{0.5}S_8$ and TlV_4FeS_8 taken at 77 K. The spectra were fitted as a superposition of three different subspectra due to the different crystallographic sites.

TABLE 4

Mössbauer Hyperfine Field Data for $Tl_{4.5}Fe_{0.5}S_8$ and TlV_4FeS_8

	$TlV_{4.5}Fe_{0.5}S_8$		TlV_4FeS_8	
	77 K	300 K	77 K	300 K
IS(1)	0.70(2)	0.56(2)	0.68(2)	0.54(2)
IS(2)	0.73(1)	0.59(1)	0.73(1)	0.59(1)
IS(3)	0.81(2)	0.67(2)	0.73(2)	0.61(2)
QS(1)	0.54(3)	0.47(3)	0.46(3)	0.46(3)
QS(2)	0.97(1)	0.87(1)	0.98(1)	0.88(1)
QS(3)	0.83(2)	0.71(2)	0.66(2)	0.61(2)
Int	23		22	
Int(2)	63		58	
Int(3)	14		20	
B_{eff}(1–3)	165(5)		147(5)	
Θ_D [K]	260(5)		260(5)	

Note. IS, isomer shift; QS, quadrupole splitting. Both are given in mm/sec relative to α-Fe. The magnitude of the internal magnetic fields B_{eff} is given in kG. Int, intensity of the spectral areas in %; Θ_D is the averaged local Debye temperature.

TABLE 5
Hyperfine Field Data for Different Iron Containing Compounds Extracted from the Literature

	IS	QS	T [K]	
FeV_2Se_4	0.67	—	—	8
$FeCr_2S_4$	0.86	—	—	26
$KFeS_2$	0.42	0.52	—	26
$FeIn_2S_4$	1.14	3.27	—	26
V_5S_8(2%^{57}Fe)	0.58	0.28	295	11
	0.64	0.67	4.2	11
$BaVS_3$(2%^{57}Fe)	0.45	1.36	295	11
	0.60	1.51	20	11
FeV_2S_4	0.57	—	295	10
	0.83	—	4.2	10
V_3S_4(1%^{57}Fe)	0.54	—	295	10
	0.83	—	4.2	10
V_4FeS_8	0.89	—	295	10
	0.71	—	4.2	10
V_5S_8(1%^{57}Fe)	0.94	—	295	10
	1.14	—	4.2	10
$Fe_{0.1}V_{0.9}S_2$	0.40	—	4.2	13
$LiFe_{0.1}V_{0.9}S_2$	0.73	—	4.2	13
$Fe_{0.1}TiS_2$	0.75	0.40	300	27
$Fe_{0.2}TiS_2$	0.73	0.53	300	27
$Fe_{0.33}TiS_2$	0.75	0.43	300	27
$Fe_{0.28}TaS_2$	0.83(3)	0.64(3)	300	28
$V_{2.5}Fe_{0.5}S_4$	0.645	0.657	300	29
	0.354	0.402	77	29
V_4FeS_8	0.520	0.348	300	29
	0.292	0.297	77	29
$Tl_{0.77}V_5FeS_8$	0.635	0.626	300	29
$Tl_{0.95}V_4FeS_8$	0.412	0.453	300	29

ance, one immediately recognizes that a one-to-one substitution of the vanadium M sites by iron, with an intensity ratio 20:40:40 for $M1$:$M2$:$M3$, does not occur. In addition, the hyperfine parameters for the subspectra with lower intensity vary slightly with the Fe content, indicating that the Fe substitution modifies somewhat the lattice sites. An assignment of the three subspectra to the M sites will be proposed after presenting the other information derived from the Mössbauer spectra.

Mössbauer spectra of TlV_4FeS_8 recorded at different temperatures are shown in Fig. 6. Down to 20 K the spectra show no magnetic effects. At around 17 K, one observes first a (relaxation-like) magnetic line broadening and then at around 10 K a magnetic splitting with strongly broadened lines. Such spectral features are reminiscent of a spin-glass behavior. The magnetic spectra were fitted again with three subspectra with site intensities and values of IS and QS derived at temperatures above 20 K. These fits reveal that there is a distribution in the angles between B_{eff} and the respective main axes of the electric field gradient as expected for a spin-glass with varying directions of the magnetic interaction with randomly substituted Fe neighbors. Since there is no unique fit of this complex problem, we fitted the magnetic spectra with only one site and obtained averaged values for the hyperfine parameters. For TlV_4FeS_8 we obtained B_{eff} = 165 kG from the spectrum taken at 1.9 K. This value can be regarded as the saturation value of B_{eff} and is, together with the values of the isomer shift, a strong argument that Fe^{3+} is present in the $S = \frac{1}{2}$ low spin state. For $TlV_{4.5}Fe_{0.5}S_8$, the value B_{eff} = 147 kG at 1.7 K seems not to be fully saturated, since here magnetic line broadening is observed to start below 10 K. In both samples, $B_{\text{eff}}(T)$ does not follow a Brillouin function for $S = \frac{1}{2}$, again pointing to a spin-glass type of the magnetic interactions, being weaker in the sample with the lower Fe content.

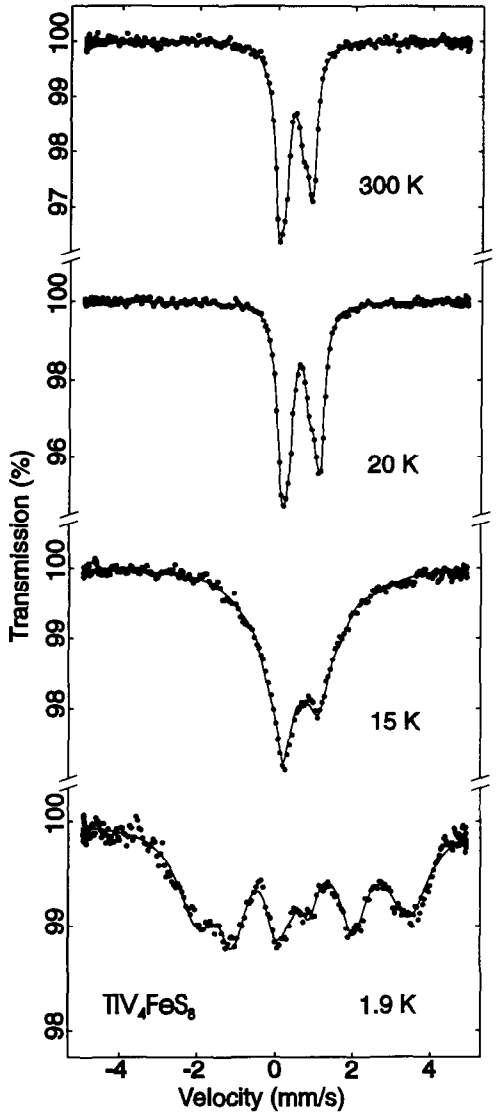

FIG. 6. Typical Mössbauer spectra of TlV_4FeS_8 as a function of temperature. The spectra display at low temperatures a magnetic transition caused by spin-glass-like behavior.

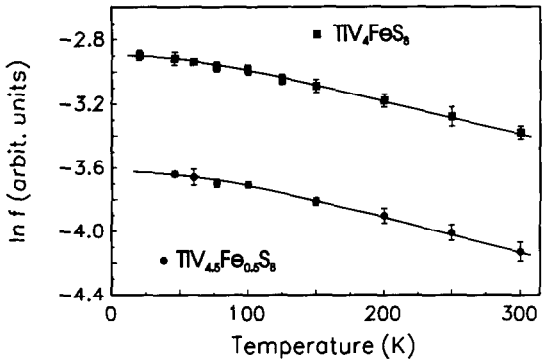

FIG. 7. Total area of the three different subspectra for both samples. In both cases one derives an averaged Debye temperature of Θ_D = 260(3) K, indicating that Fe doping does not influence the bond strength of iron on the different sites.

We have evaluated in detail the temperature dependence of hyperfine parameters and intensities of the three quadrupole spectra between 45 and 300 K. All data show the normal temperature dependence expected for Fe^{3+} ions. The quadrupole interactions decrease continuously by about 15% within this temperature range. The relative site intensities vary slightly with temperature. We derive from a Debye fit of the spectral areas local Debye temperatures of Θ_D (M1–3) = 220(7), 265(5), and 262(15) K, respectively. The change of the total area with temperature is depicted in Fig. 7. For the total area of the three subspectra, we derive for both samples Θ_D = 260(3) K. With the local Debye temperatures and the relative site intensities, we calculated the site intensities of the three subspectra given in Table 4.

For the assignment of the three subspectra to the M1–M3 sites one can use at first the magnitude of the quadrupole splittings. It can be argued that a more regular environment causes a smaller quadrupole splitting. As shown by the crystallographic data (see Table 2) the M1 sites are within the most regular sulfur octahedron (δ = 0.006 and 0.003 Å), which should result in the smallest quadrupole splitting, here the doublet with QS(1). The distortion of the two other MS_6 octahedra is considerably larger and comparable in magnitude (δ = 0.233 Å for M2 and δ = 0.22 Å for M3). We argue from the crystallographic data of Table 1 that the most intense subspectrum with the largest quadrupole splitting, QS(2), originates from Fe^{3+} on M2 sites. The $M(2)S_6$ octahedra connect the sheets built up from M1 and M3 centered octahedra via common faces and influence mostly the b-axis of the lattice. It is the b-axis which exhibits the largest variation upon Fe substitution or Tl intercalation. The observed increase of the b-axis with Fe substitution can be understood as being due to less pronounced attractive M2–M2 interactions. Such a behavior explains also the net increase in the unit cell dimensions despite the smaller ionic radius of Fe^{3+} in comparison to V^{3+}. This preferential site occupation of the M2 site is more pronounced for the Fe-poorer sample.

4. CONCLUSIONS

In summary, we have demonstrated that the substitution of V by Fe in $TlV_{5-y}Fe_yS_8$ results in an increase of the lattice parameters. This surprising result cannot be explained on the basis of the different ionic radii for V^{3+} and Fe^{3+}. The analysis of the crystallographic data show that the average $\langle M\text{–S}\rangle$ distances are only slightly affected by the substitution but considerable differences are observed for the distortion of the MS_6 octahedra, as is shown by the alterations of the asymmetry δ. In addition significant changes are observed for the different M–M interatomic separations. With raising Fe content the M–M distances increase. Since the $\langle M\text{–S}\rangle$ distances show only minute changes the observed increase of the lattice parameters is attributed to changes of the M–M interactions, which become less strong with increasing Fe content. This interpretation is in line with the smaller spatial extension of the radial part of the 3d wave functions of Fe compared with that of V. As a consequence the orbital overlap between neighbored M atoms and therefore the bond strength become less strong with raising Fe content.

The reaction of TlV_4FeS_8 with I_2 in CH_3CN not only removes the Tl atoms but also results in a considerable attack of the redox agent on the host material. This finding clearly demonstrates that the substitution of V by Fe leads to pronounced changes of the electronic structure of the material since no reaction between the host and I_2 was observed for TlV_5S_8 (15, 20).

The changes of the interatomic separations with decreasing Tl abundance can be understood only on the basis of predominantly electronic factors, i.e, the oxidation of some of the M^{3+} ions to M^{4+}.

The magnetic properties of $TlV_{5-y}Fe_yS_8$ (y = 0.5 and 1.0) are explained on the basis of the coexistence of a temperature-independent paramagnetism and a Curie–Weiss-like contribution. The evaluated local magnetic moment is in agreement with a Fe^{3+} species in the low spin sate. A strong increase of the TIP is obtained for the Fe-richer sample indicative of an appreciable delocalization of Fe 3d electron density. This delocalization happens despite the longer M–M interatomic distances compared to the Fe-poorer compound. Furthermore, this result suggests that the enlargement of the M–M distances does not lead to the "isolation" of the M ions but maintains the delocalized character of the compound.

The Mössbauer hyperfine field parameters give strong evidence for the existence of Fe^{3+} in the low spin state. In addition, the Fe atoms substitute the V atoms not in

a random fashion but show a site preference for the $M2$ site. Below about 20 K the magnetic moments in TlV_4FeS_8 start to order. The change of the spectral features with temperature are typical for spin-glass behavior. The evaluated value for the effective field at 1.9 K of B_{eff} = 165 kG can be regarded as the saturation value of B_{eff} for Fe^{3+} in the low spin state. For the Fe-poorer sample a magnetic ordering occurs at a clearly lower temperature of about 10 K. Here, the B_{eff} of 147 kG evaluated at 1.7 K seems not to be fully saturated. For both compounds B_{eff} vs T does not follow the Brillouin function for a $S = \frac{1}{2}$ spin system, which again is an indication of spin-glass behavior of the local magnetic moments. For both samples average Debye temperature Θ_D = 260(3) K indicates that there are no significant differences of the stiffness of the two Fe-substituted samples.

ACKNOWLEDGMENTS

Financial support by the Deutsche Forschungsgemenschaft (DFG) as well as by the Fonds der Chemischen Industrie is gratefully acknowledged. Special thanks to Dr. W. Biberacher (Walther-Meissner Institut Garching), who has performed the electrical resistivity measurements.

REFERENCES

1. T. Ohtani and S. Onoue, *Mater. Res. Bull.* **21,** 69 (1986).
2. W. Schramm, R. Schöllhorn, H. Eckert, and W. Müller-Warmuth, *Mater. Res. Bull.* **18,** 1283 (1983).
3. W. Bensch, E. Amberger, and J. Abart, *Solid State Commun.* **51,** 979 (1984).
4. W. Bensch, J. Abart, E. Amberger, H. W. Schmalle, and J. Kopf, *Acta Crystallogr. Sect. C* **42,** 6 (1986).
5. W. Bensch, E. Wörner, and U. Ruschewitz, *J. Solid State Chem.* **110,** 234 (1994).
6. W. Bensch, E. Wörner, M. Muhler, and U. Ruschewitz, *Eur. J. Solid State Inorg. Chem.* **30,** 645 (1993).
7. W. Bensch, E. Wörner, and F. Tuczek, *Mater. Res. Bull.*, in press.
8. H. N. Ok and C. S. Lee, *Phys. Rev. B* **29,** 5168 (1984).
9. H. Nozaki, H. Wada, and H. Yamamura, *Solid State Commun.* **44,** 63 (1982).
10. Y. Oka, K. Kosuge, and S. Kachi, *Mater. Res. Bull.* **12,** 1117 (1977).
11. O. Massenet, J. Mercier, A. Chang, R. Buder, and A. B. H. Mohamed, *J. Phys. Chem. Solids,* **41,** 1009 (1980).
12. K. S. Baek, Y. S. Park, and H. N. Ok, *Phys. Rev. B* **30,** 404 (1984).
13. F. J. DiSalvo, M. Eibschütz, C. Cros, D. W. Murphy, and J. V. Waszczak, *Phys. Rev. B* **19,** 3441 (1979).
14. M. Eibschütz and F. J. DiSalvo, *Phys. Rev. Lett.* **36,** 104 (1976).
15. W. Bensch and E. Wörner, *Solid State Ionics* **58,** 275 (1992).
16. R. D. Shannon, *Acta Crystallogr. Sect. A* **32,** 751 (1976).
17. R. D. Shannon, *in* "Structure and Bonding in Crystals, Vol. II" (M. O'Keeffe and A. Navrotsky, Eds.). Academic Press, San Diego, 1981.
18. W. Bensch, O. Helmer, and F. Tuczek, in preparation.
19. K. Vidyasagar and J. Gopalakrishnan, *J. Solid State Chem.* **42,** 217 (1982).
20. E. Wörner and W. Bensch, *Beitr. Elektronenmikroskop. Direktabb. Oberfl.* **25,** 173 (1992).
21. H. Nozaki and H. Wada, *J. Solid State Chem.* **47,** 69 (1983).
22. P. Terzieff, *Monatsh. Chem.* **109,** 657 (1978).
23. P. Terzieff and K. L. Komarek, *Monatsh. Chem.* **109,** 651 (1978).
24. S. Muranaka and T. Takada, *J. Solid State Chem.* **14,** 291 (1975).
25. L. B. Morris, R. H. Plovnick, and A. Wold, *Solid State Commun.* **7,** 291 (1969).
26. N. N. Greenwood and H. J. Whitfield, *J. Chem. Soc. A,* 1697 (1968).
27. M. Inoue, M. Matsumoto, H. Negishi, and H. Sakai, *J. Magn. Mater.* **53,** 131 (1985).
28. M. Eibschütz, F. J. DiSalvo, G. W. Hull, Jr., and S. Mahajan, *Appl. Phys. Lett.* **27,** 464 (1975).
29. W. Bensch, R. Schlögl, and E. Amberger, *Helv. Chim. Acta* **69,** 35 (1986).